Bombesin functionalized gold nanoparticles show in vitro and in vivo cancer receptor specificity

Nripen Chanda[a], Vijaya Kattumuri[b], Ravi Shukla[a], Ajit Zambre[a], Kavita Katti[a], Anandhi Upendran[c], Rajesh R. Kulkarni[a,d], Para Kan[e], Genevieve M. Fent[f], Stan W. Casteel[f], C. Jeffrey Smith[a,g,h], Evan Boote[a], J. David Robertson[d,e,h], Cathy Cutler[d,e,h], John R. Lever[a,g,i], Kattesh V. Katti[a,b,c,h,1], and Raghuraman Kannan[a,c,1]

Departments of [a]Radiology and [b]Physics, [d]Nuclear Science and Engineering Institute, Departments of [e]Chemistry, [f]Veterinary Pathobiology, and [i]Medical Pharmacology and Physiology, [g]Harry S. Truman Veterans Administration Medical Center, and [h]Missouri University Research Reactor, University of Missouri, Columbia, MO 65212; and [c]Nanoparticle Biochem Inc., Columbia, MO 65211

Communicated by M. F. Hawthorne, University of Missouri, Columbia, MO, March 2, 2010 (received for review November 23, 2009)

Development of cancer receptor-specific gold nanoparticles will allow efficient targeting/optimum retention of engineered gold nanoparticles within tumors and thus provide synergistic advantages in oncology as it relates to molecular imaging and therapy. Bombesin (BBN) peptides have demonstrated high affinity toward gastrin-releasing peptide (GRP) receptors in vivo that are overexpressed in prostate, breast, and small-cell lung carcinoma. We have synthesized a library of GRP receptor-avid nanoplatforms by conjugating gold nanoparticles (AuNPs) with BBN peptides. Cellular interactions and binding affinities (IC_{50}) of AuNP–BBN conjugates toward GRP receptors on human prostate cancer cells have been investigated in detail. In vivo studies using AuNP–BBN and its radiolabeled surrogate ^{198}AuNP–BBN, exhibiting high binding affinity (IC_{50} in microgram ranges), provide unequivocal evidence that AuNP–BBN constructs are GRP-receptor-specific showing accumulation with high selectivity in GRP-receptor-rich pancreatic acne in normal mice and also in tumors in prostate-tumor-bearing, severe combined immunodeficient mice. The i.p. mode of delivery has been found to be efficient as AuNP–BBN conjugates showed reduced RES organ uptake with concomitant increase in uptake at tumor targets. The selective uptake of this new generation of GRP-receptor-specific AuNP–BBN peptide analogs has demonstrated realistic clinical potential in molecular imaging via x-ray computed tomography techniques as the contrast numbers in prostate tumor sites are severalfold higher as compared to the pretreatment group (Hounsfield unit = 150).

gold nanoparticles | bombesin | gastrin-releasing peptide receptor | prostate cancer | computed tomography imaging

A recent study involving 77,000 North American men has shown that regular prostate specific antigen (PSA) screening did not save a significant number of lives over 10 y (1). Early detection of prostate tumors by computed tomography (CT), ultrasound, MRI, or PET/single photon emission CT (SPECT) imaging modalities is often inaccurate and more complex as the prostate is deep inside the pelvis and hard to access (2–5). Indeed, there is a clinical need for highly accurate detection modalities for the patient community at risk for developing prostate cancer.

The nanomedicine approach uses targeted nanoparticles as platforms to design imaging probes and therapeutic agents for cancer and other human disorders (6, 7). In particular, nanoparticles of gold have already demonstrated "proof of concept" for diagnosis and therapy of various different types of cancers and thus present realistic potential for clinical translation (8–12). On the molecular imaging front, gold with a K-edge at 80.7 keV has higher absorption than iodine (K-edge at 33 keV), thus minimizing bone and tissue interference, which results in better contrast with a lower x-ray dose (13). Our extensive in vivo studies (in mice, pigs, and dogs) have confirmed that gold nanoparticles (AuNPs) show significantly higher x-ray absorption characteristics than iodinated CT agents (8, 9, 14, 15). Recently, Kopelman and co-workers have demonstrated the feasibility of using targeted AuNPs embedded in cancer cells for CT imaging under in vitro conditions (16). Despite considerable progress achieved to date toward the development of target-specific AuNPs for use in early cancer detection, a vast majority of these systems perform well only under in vitro profiles and fail to maintain target specificity/efficacy under in vivo conditions (17).

Target specificity is achieved through hybrid nanoparticles that are produced by conjugating AuNPs with tumor-specific biomolecules, including monoclonal antibodies, aptamers, peptides, or various receptor-specific substrates (9, 18). In this study, we present a unique bioconjugation approach that affords the synthesis of a library of AuNPs conjugated with gastrin-releasing peptide (GRP) receptor-avid bombesin (BBN) for targeting GRP receptor sites overexpressed in prostate tumors. Here, we present our detailed investigations encompassing the following: (*i*) the bioconjugation chemistry involving the development of a library of GRP receptor-avid AuNP–BBN conjugates; (*ii*) GRP receptor specificity and binding affinity including IC_{50} evaluations of AuNP–BBN conjugates under in vitro conditions with PC-3 cells using radioiodinated bombesin displacement assays; (*iii*) results on in vivo GRP receptor targeting efficacy and optimum delivery modes (i.v., intratumoral vs. i.p.) of AuNP–BBN in normal and prostate-tumor-bearing mice; and (*iv*) efficacy of AuNP–BBN nanoplatforms as x-ray contrast agents for molecular CT imaging of prostate tumors in mice.

Results and Discussion

The development of cancer receptor-specific AuNPs will have measurable impacts on the future of nanoparticle-based molecular imaging and therapy and on the overall field of oncology. As part of our ongoing efforts toward the development of tumor-specific gold nanoparticles, we chose conjugations of AuNPs with BBN peptide analogs because this peptide library has demonstrated high affinity toward GRP receptors in vivo (overexpressed in prostate, breast, and small-cell lung carcinoma). Schally and co-workers have shown that there are 44,000 bombesin receptor sites on human prostate cancer (PC-3) cells (19). A number of clinical trials in progress are using BBN peptide analogs to target GRP receptors present in prostate cancer for imaging applications (20). In a human phase-1 clinical study involving radioactive ^{99m}Tc-BBN, the radioactivity was found within 4 min post injection in the prostate tumor region (20). In another human clinical study involving 10 prostate tumor patients, who were injected with 185 MBq of ^{99m}Tc-BBN with Gleason's score levels of 7.5 (±1.3), targeting accuracy and sensitivity of BBN peptides in imaging GRP receptor overexpressing

Author contributions: K.V.K. and R.K. designed research; N.C., V.K., R.S., A.Z., K.K., A.U., and K.V.K. performed research; R.R.K., P.K., G.M.F., S.W.C., C.J.S., E.B., J.D.R., C.C., G.L.S., and K.V.K. contributed new reagents/analytic tools; N.C., R.S., A.Z., K.K., A.U., C.J.S., C.C., J.R.L., R.K., and K.V.K. analyzed data; and N.C., K.V.K., and R.K. wrote the paper.

The authors declare no conflict of interest.

[1]To whom correspondence may be addressed. E-mail: kattik@health.missouri.edu or kannanr@health.missouri.edu.

This article contains supporting information online at www.pnas.org/cgi/content/full/1002143107/DCSupplemental.

prostate tumors has been confirmed. In this study, two patients exhibiting higher PSA levels (>20 ng/mL) showed high uptake of radioactivity in prostate tumors 1 min post injection. These human clinical trials data confirm that BBN-labeled imaging agents can be used for imaging and staging prostate cancers (21). The proven propensity of BBN peptide analogs in providing receptor-targeting specificity when conjugated with diagnostic probes prompted us to test the hypothesis that BBN conjugated with ^{198}AuNPs would deliver diagnostic/therapeutic payloads with high specificity to GRP receptors overexpressed in prostate cancer. We also hypothesized that tumor-specific AuNP–BBN will induce appropriate x-ray contrast to detect GRP-receptor–expressing prostate tumors under in vivo conditions. Details of bioconjugation of AuNPs with BBN peptide, in vivo targeting ability, and CT imaging efficacy of AuNP–BBN conjugates in prostate-tumor-bearing mice are described in the sections that follow.

Bioconjugation of AuNPs with Bombesin Peptide. Our synthetic protocol utilizes starch stabilized AuNPs (SAuNPs) and thioctic-acid-linked truncated GRP receptor-avid bombesin peptide as synthons for the generation of AuNP–BBN conjugates (Scheme 1). Thioctic acid contains a disulfide group to bind AuNPs and a carboxylic acid group to conjugate with bombesin peptide. Note that the availability of reactive sites on the surface of AuNPs allows the incorporation of varying amounts of BBN peptides and provides a practical means of developing a library of AuNP–BBN conjugates (AuNP–BBN-1, AuNP–BBN-2, or AuNP–BBN-3; Scheme 1). Size measurements on AuNP–BBN have inferred that the particles are spherical in shape within the core size range of ~16–18 nm (Table 1). Particle distribution analysis of AuNP–BBN conjugates confirms that particles are uniformly dispersed with a hydrodynamic diameter of 115–155 nm, suggesting that bombesin molecules are conjugated to AuNPs. The increase in hydrodynamic diameter from AuNP–BBN-1 to AuNP–BBN-3 confirms the presence of increased amounts of BBN peptide. These results are corroborated using disc centrifuge analysis measurements (Table 1 and *SI Materials and Methods*).

The starch molecules that encapsulate AuNPs remain bound to the nanoparticle surface through electrostatic interactions even after conjugation with bombesin peptide. The larger hydrodynamic size of AuNP–BBN conjugates (Table 1) strongly supports the coexistence of starch and BBN units bound to the gold surface. X-ray photoelectron spectroscopic (XPS) data (*SI Materials and Methods*) provide conclusive experimental evidence for the presence of starch molecules within the AuNP–BBN framework. Detailed structural investigations of starch molecules reveal a combination of both lamellar and fibrous networks, which are composed of spherical blocklets 400–500 nm in diameter (22, 23). The average size of a bombesin peptide used in the present study is around 2–3 nm. Because of the inherent structural porosity of starch layers bound to the AuNP surface, bombesin peptides can access the surface of gold nanoparticles by partially dislodging starch encapsulants.

In vitro stability studies of AuNP–BBN conjugates were conducted by incubating with solutions of 10% NaCl, 0.5% cysteine, 0.2 M histidine, 0.5% human serum albumin, 0.5% BSA, or 0.2 M DTT. The stability of the nanoconjugates at different time points was analyzed by monitoring the plasmon resonance using UV-visible spectroscopy (UV-Vis; *SI Materials and Methods*). Our experiments reveal that AuNP–BBN-1 and AuNP–BBN-2 are unstable and tend to aggregate in these solutions. However, AuNP–BBN-3 showed remarkable stability in all of the above solutions as the plasmon resonance absorption and bandwidth remained unaltered for 24 h. These in vitro stability data indicate that gold sulfur bonds within AuNP–BBN-3 have optimum kinetic stability for use in subsequent receptor-targeting applications under in vivo profiles. The negative zeta potential value of −27.2 mV for AuNP–BBN-3 indicates that the particles repel each other and that there is no tendency for the particles to aggregate. Therefore, AuNP–BBN-3 was chosen for detailed in vivo prostate tumor targeting and molecular imaging investigations.

Evaluation of in Vitro GRP Receptor Binding Affinity of AuNP–BBN Constructs. Human prostate tumor PC-3 cells exhibit a large number of GRP receptors on the surface of the cells. The binding affinity (IC_{50}) of AuNP–BBN conjugates has been evaluated by competitively displacing radioiodinated bombesin ^{125}I-Tyr^{4}BBN from the surface of PC-3 cells. A plot of PC-3 cell-bound radioactive bombesin versus the increased concentrations of AuNP–BBN conjugates has been used to determine IC_{50} values (*SI Materials and Methods*). The IC_{50} values for the conjugates are reported in micrograms because the molecular weights of the gold conjugates cannot be accurately determined. It is evident from the data that the IC_{50} values or cell-binding affinity of conjugates depend on the degree of BBN peptide coated over AuNPs. AuNP–BBN-3, which has more bombesin peptides on the surface, exhibits a lower IC_{50} value (or a higher cell-binding affinity) when compared with other conjugates (Table 1).

Generation of Radioactive Surrogate ^{198}AuNP–BBN-3 for in Vivo Investigations. Although a myriad of analytical methods are effective in estimation of gold in various organs, accurate quantification and understanding of pharmacokinetics of AuNPs can be achieved efficiently by radiolabeling gold with ^{198}Au because the sensitivity of

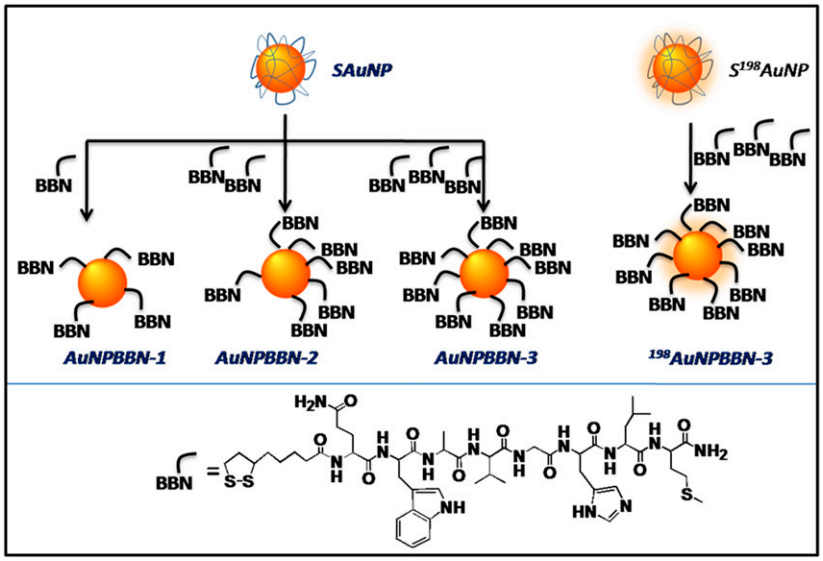

Scheme 1. Schematic of synthesis of AuNP–BBN and ^{198}AuNP–BBN conjugates (*Upper*) and amino acid sequence in thioctic acid–bombesin peptide (*Lower*). The available reactive sites on AuNPs allow incorporation of varying amounts of BBN peptides and provide a practical means of developing a library of AuNP–BBN analogs with one-, two-, and three-peptide equivalents per nanoparticle, resulting in AuNP–BBN-1, AuNP–BBN-2, and AuNP–BBN-3 for low/high capacity binding with GRP receptors.

Table 1. Solubility, size, charge, and GRP receptor binding affinity of AuNP–BBN conjugates

Sample	Solubility (mg/mL)	Size (nm) TEM	CPS	DLS	Zeta potential (mV)	IC_{50} (μg/mL) with PC-3
Au–BBN-1	5	16 ± 7	70	115	−23.4	8.10 ± 0.30
Au–BBN-2	5	16 ± 5	117	137	−26.2	3.37 ± 0.44
Au–BBN-3	<3	16 ± 5	125	155	−27.2	2.45 ± 0.18

scintigraphic radio-counting methods exceeds all other analytical techniques. This sensitivity is of profound importance as the amounts of nanoparticles to be estimated in tissue/blood/urine and other important organs would be in sub-nano/pico molar levels. Radioactive ^{198}Au is a medium-energy β-emitter (β max = 0.96 MeV; $t_{1/2}$ = 2.7 d with a γ-radiation at 0.411 MeV) (24). Radiolabeling experimental drugs without altering the chemical backbone is always considered to be the most promising modality and a well-accepted practice for predicting the in vivo biodistribution and the overall pharmacokinetic profiles. In view of these considerations, in the present study, we have used ^{198}AuNP–BBN as radioactive surrogates for AuNP–BBN conjugates. The radioactive surrogate of AuNP–BBN-3 was synthesized using S^{198}AuNP and thioctic-acid–bombesin peptide as starting materials. (see Scheme 1).

Optimum Modes of AuNP–BBN Administration. It is well known that administration of nanoparticles via i.v. mode in small or large animals results in opsonization followed by substantial uptake by macrophages present in liver and spleen. Consequently, the concentration of nanoparticles in the desired target organs would be significantly less than required for specific molecular imaging/therapy applications. To circumvent these problems associated with reticuloendothelial system (RES) uptake of drugs, the s.c. mode of delivery has been tried (25). However, the s.c. mode of delivery results in slower tissue distribution kinetics, which restricts the mobility of drugs to target organs. We have investigated the possibility of using the i.p. mode of administration to populate the drug in the abdominal cavity with the hope that the tumor-specific nanoparticles would reach the diaphragm before being absorbed by lymphatic capillaries. The overall rationale has been to provide increased chances for the nanoconjugates to interact with target receptors before they interact with macrophages present in liver and spleen. Recently, it has been shown that the i.p. mode of delivery of chitosan/siRNA nanoconjugates provides the maximum therapeutic benefit as compared to the i.v. or s.c. modes of administration (26). Sawicki and Anderson have demonstrated the effectiveness of the i.p. mode of administration of polymeric nanoparticles to tailor delivery of DNA to encode diphtheria suicide protein for the treatment of advanced stage ovarian cancer (27). Indeed, there are several examples in the literature that illustrate the efficacy of the i.p. mode of injection of using liposomes and polymeric nanoparticles in attaining maximum therapeutic benefits (molecular therapy) (26). Of relevance to our study, Danscher and co-workers have examined the tissue distribution kinetics of AuNPs after delivering them via i.v. and i.p. modes (28). Their studies have shown that the i.p. mode of administration resulted in minimal uptake of AuNPs by Kupffer cells in liver as compared to the i.v. mode of administration (28). Motivated by these findings, we have investigated administration of GRP-receptor-specific AuNP–BBN-3 via i.p. mode and evaluated the uptake of nanoparticles in RES organs and GRP-receptor–expressing organs. As discussed above, mice serve as ideal animal models because they possess a reservoir of GRP receptors in pancreatic acini. Normal mice provide an approximately eightfold higher GRP receptor density in pancreas than in prostate tumors; therefore, normal CF-1 mice were injected with AuNP–BBN-3 conjugates via i.p. mode and the concentration of nanoparticles in RES organs and pancreas was estimated. In this study, the animals were euthanized 3 h after the AuNP–BBN-3 injection period.

As shown in Fig. 1, the i.p. mode of administration of AuNP–BBN-3 resulted in 0.3 ppm of gold in liver, which is among the lowest levels of uptake of gold in nontarget organs as compared to all previously known AuNP–peptide conjugates. Indeed, the GRP-receptor-specific uptake of AuNP–BBN-3 in pancreas reached 9.3 ppm (Fig. 1), thus demonstrating that the i.p. mode of delivery circumvents problems associated with RES uptake

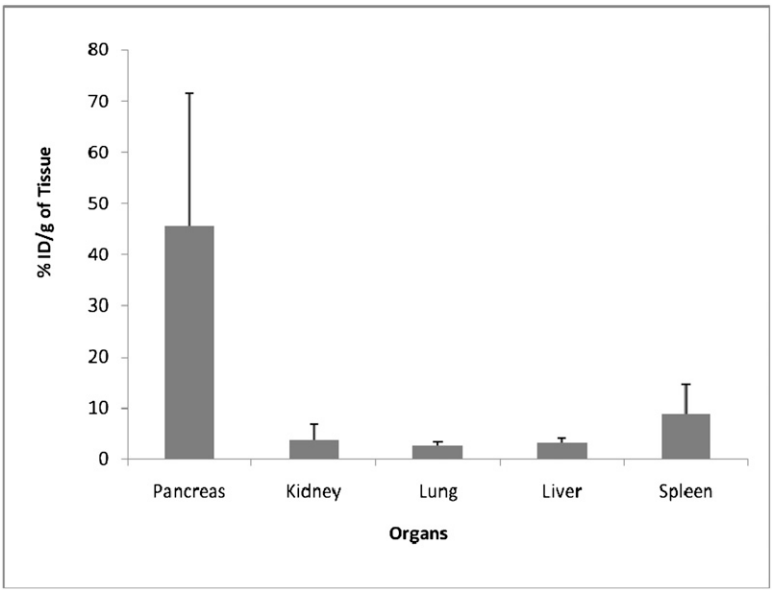

Fig. 1. Concentrations of gold in various organs after i.p. injection of AuNP–BBN-3 in normal mice. It is important to note that the i.p. mode of injection decreases the RES organ uptake of AuNPs while maximizing GRP-receptor–mediated uptake in desired sites.

and navigates nanoparticles efficiently and selectively to GRP receptors present in acinar cells in the pancreas that are accessible to the blood stream. Our findings convincingly demonstrate that the i.p. mode of delivery provides excellent in vivo targeting opportunities for using the ability of AuNP–BBN conjugates to target GRP-receptor–expressing cells for molecular imaging and therapy of prostate and other GRP-receptor-positive tumors.

Evaluation of in Vivo GRP Receptor Binding Affinity of ^{198}AuNP–BBN-3 Nanoconstructs. The GRP-receptor-targeting efficacy of ^{198}AuNP–BBN-3 was investigated by injecting the nanoconjugate via i.p. in prostate tumor bearing severe combined immunodeficient (SCID) mice models. The animals were killed at 30 min and 1, 2, 4, and 24 h post injection, and radioactivity in both target and nontarget organs was counted (Fig. 2). The GRP-receptor density in mice is in the following order: pancreas > tumor > intestine (29). A recent study has quantified that more than ~300 ($\times 10^3$) bombesin receptor sites per cell are available in mice pancreas and that prostate tumor PC-3 cells have ~44 ($\times 10^3$) receptor sites per cell (30). These data imply that GRP-receptor density in pancreas is approximately eightfold higher than that in PC-3 tumors. In addition, the wealth of data available in the literature on the biodistribution and tumor uptake/localization of GRP receptor–avid bombesin-like peptides labeled with PET or SPECT radionuclides indicates that the accumulation of peptide-tagged radiotracers is always higher in intestines than in tumors due to higher blood flow in the intestines as compared to that of tumor tissue (20, 21, 29, 30). Indeed, our results clearly demonstrate that the biodistribution of ^{198}AuNP–BBN-3 follows a similar trend. We have observed a predominant uptake of ^{198}AuNP–BBN-3 conjugates in GRP-receptor–expressing pancreatic acini [56.7% injected dose/gram (ID/g) after 4 h] and with 0.48% ID/g in tumors in prostate-tumor-bearing mice. The uptake of radioactivity in the pancreatic tissue increased over the post-injection period, reaching a maximum at 4 h with slow clearance beyond 12 and 24 h (Fig. 2). After 24 h, the level of ^{198}Au activity was as low as what was seen at 30 min post injection (15.9% ID/g; Fig. 2), thus indicating significant clearance from the pancreatic region. There was a definite uptake of ^{198}AuNP–BBN-3 within prostate tumors, although it was significantly lower than in pancreas as expected per the eightfold higher GRP receptor density within pancreas as compared to prostate tumors. The lower uptake of ^{198}AuNP–BBN in tumor may be a consequence of the heterogeneity of tumor tissue as compared to the highly homogenic pancreatic organ.

Our results concerning the selective uptake of AuNP–BBN within GRP receptors in pancreas/prostate tumors represent previously undescribed examples of the targeted delivery of AuNPs and are consistent with the GRP-receptor uptake and pharmacokinetics data previously reported for a number of ^{99m}Tc-bombesin and other radio-trace–labeled conjugates in mice models. For example, ^{99m}Tc $(H_2O)(CO)_3$-Dpr-(SSS)-BBN[7-14]NH_2 showed an uptake of 23.3% ID/g and 10.2% ID/g in pancreas and intestines, respectively, 1 h post injection (31), whereas ^{99m}Tc(litorin) showed 23.56% ID/g in pancreas 30 min post injection (32). ^{177}Lu-DOTA-8-Aoc-BBN[7-14]NH_2 has shown 38.5% ID/g in pancreas and 5.60% ID/g in intestines (33). The slower uptake of ^{198}AuNP–BBN-3 nanoparticles in kidney (2.46% ID/g after 4 h and 1.58% ID/g after 24 h) suggests that smaller nanoconjugates (^{198}AuNP-BBN-3 <5 nm) are excreted through either the urinary or the hepatobiliary pathway. ^{198}AuNP-BBN-3 conjugates were also cleared from the blood via the RES by accumulation in liver and spleen. It is evident from the pharmaco-

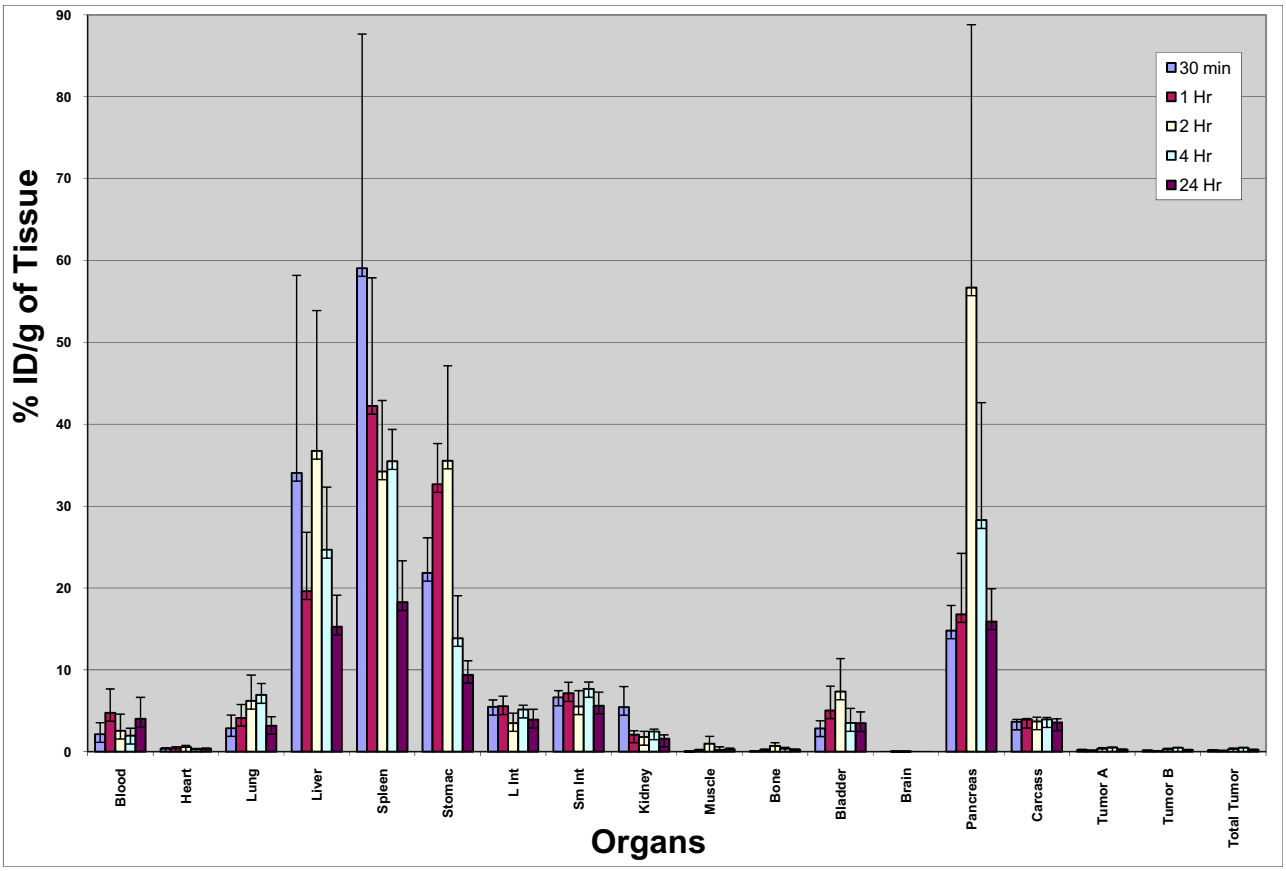

Fig. 2. Concentrations of ^{198}AuNP–BBN-3 conjugates in various organs after i.p. injection in prostate-tumor-bearing mice models. The uptake of nanoparticles at 30 min and 1, 2, 4, and 24 h post injection was measured. A significant receptor-mediated uptake of ^{198}AuNP–BBN-3 conjugates in GRP-receptor–expressing pancreatic acini (56.7% ID/g after 4 h) was observed. Note that the GRP-receptor density in mice is in the following order: pancreas > tumor > intestine.

kinetic data on AuNP–BBN-3 that the spleen shows a higher uptake than the liver, which can be attributed to the higher filtering efficacy of the spleen.

A number of detailed studies on the interrelationships of pharmacokinetics and nanoparticulate sizes and the tumor-targeting ability of polymeric and liposome-based nanoparticles indicate that larger nanoparticles show slower clearance from blood and higher uptake in liver and spleen. These results have been rationalized on the basis of the size match of the nanoparticles with liver fenestrae, which results in higher penetration in the endothelial walls of liver (25). The enhanced uptake in RES organs is due to the presence of a high degree of phagocytic cells and also to the capillary beds in both the organs. In addition, two independent studies on size-dependent pharmacokinetics and plasma clearance of PEGylated AuNPs have recently confirmed that smaller AuNPs (~20–50 nm) clear rapidly from blood with minimum RES organ uptake whereas larger nanoparticles are retained in the blood for longer periods with eventual clearance through RES organs (34). In the present study, we have shown that AuNP–BBN-3 has a core size of ~16 nm and a hydrodynamic size of ~155 nm. Based on this size profile, AuNP–BBN-3 is expected to show higher uptake in liver and spleen. However, on the contrary, our current findings have shown significantly reduced uptake of ^{198}AuNP–BBN-3 in liver (25–30% ID/g) as compared to that of 80-nm AuNP–PEG (50% ID/g uptake in liver) (34). This significant reduction of liver uptake as observed for ^{198}AuNP-BBN-3 may be rationalized in terms of the increased receptor-mediated uptake of ^{198}AuNP-BBN-3 in GRP receptors that are overexpressed in pancreas and prostate tumors.

Specific Versus Nonspecific Receptor-Mediated Uptake. To further probe the role of the AuNP–BBN conjugate as a GRP-receptor-specific candidate, a nonspecific agent such as gum Arabic protein functionalized AuNPs (GA-^{198}AuNP) (8), which have no affinity to GRP receptors, were injected in prostate-tumor-bearing mice, and the results of accumulation of gold in GRP receptor-avid pancreatic tissue were compared with those obtained from similar studies using the GRP-receptor-specific ^{198}AuNP–BBN-3 conjugate. It is important to recognize that the GA-^{198}AuNP conjugate is an excellent comparison standard as this nonspecific nanoparticulate agent possesses comparable size characteristics (core size: 13 nm; hydrodynamic size: 85 nm) to that of the target-specific ^{198}AuNP–BBN-3 conjugate. Detailed in vivo studies using GA-^{198}AuNPs showed very high uptake in liver (93.26% ID/g) 2 h post injection (Fig. 3). These results provide unequivocal evidence that the significant uptake of ^{198}AuNP–BBN-3 (Fig. 2) in pancreatic acini and within the tumors in prostate-tumor-bearing SCID mice are indeed mediated through GRP receptors, and therefore ^{198}AuNP–BBN is a reliable vector for targeting GRP receptors that are overexpressed in a host of cancer types including prostate cancer, HER+ breast cancer, and small-cell lung carcinoma. The relative accumulation of ^{198}AuNP–BBN-3 and GA-^{198}AuNP in spleen and liver, respectively, may provide significant details on the receptor targeting ability and subsequent clearance from nontarget organs. The nontargeted GA-^{198}AuNPs showed significantly higher uptake in RES organs as compared to the targeted ^{198}AuNP–BBN-3 analog, suggesting that GRP receptor targeting minimizes RES organ uptake. Our detailed pharmacokinetics and biodistribution studies on the comparison of GRP-targeted ^{198}AuNP–BBN-3 with the nontargeted GA-^{198}AuNP nanoconjugate have provided the following important insights: (*i*) ^{198}AuNP–BBN-3 exhibits excellent in vivo GRP-receptor-targeting efficacy; (*ii*) the percentage of ID/g uptake in prostate tumors has been found to be an order of magnitude higher than ^{99m}Tc-bombesin and other radio-trace–labeled conjugates in mice models; (*iii*) GRP-receptor targeting characteristics of ^{198}AuNP–BBN-3 results in a concomitant lower uptake in nontarget organs, including liver and spleen as compared to the nontargeted GA-^{198}AuNP nanoconjugate where uptake in spleen and liver is the predominant mode of clearance.

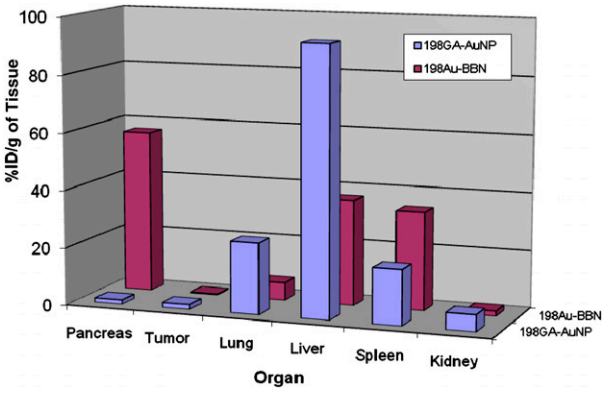

Fig. 3. Comparison of uptake of ^{198}AuNP–BBN-3 and ^{198}GA–AuNP conjugates in various organs after i.p. injection in prostate-tumor-bearing mice models. The nontargeted GA-^{198}AuNPs showed very high uptake in liver (93.26% ID/g) 2 h post injection whereas there is significant GRP-receptor–mediated uptake of ^{198}AuNP–BBN in pancreatic acini and within the prostate tumors.

Evaluation of CT Imaging Efficacy of Targeted Nanoparticles in Mice Models. Selective delivery of AuNPs at tumor sites can be used to induce clinically significant x-ray contrast to detect GRP-receptor–expressing prostate tumors for molecular imaging applications. To determine the efficacy of AuNP–BBN-3 as a targeted x-ray contrast agent for imaging prostate cancer, the following experiments were performed in nude mice bearing human prostate tumor (PC-3) xenografts: (*i*) measurement of CT numbers in tumor before treatment; (*ii*) monitoring of changes in CT numbers in tumor after injecting AuNP–BBN-3 via i.p. mode at various time points; and (*iii*) further monitoring of changes in CT numbers after injecting AuNP–BBN-3 via i.v. mode at various time points. The change in x-ray CT numbers before and after pretreatment of AuNP–BBN-3 is shown in Fig. 4. From our detailed discussions of in vivo biodistribution study outlined in previous sections, we anticipated a significant CT number change upon injecting AuNP–BBN-3 via i.p. mode due to the preferential localization of AuNP–BBN-3 in GRP-receptor–expressing PC-3 tumors. As shown in Fig. 4, the change in CT numbers at the prostate tumor site, after injecting AuNP–BBN-3 via i.p. mode, is severalfold higher than that of the pretreatment group [ΔHU (Hounsfield units) = ~150]. Clinically imageable contrast was retained beyond 6 h post injection. The contrast numbers were reduced to 63 (ΔHU) at 24 h presumably due to moderate efflux rates of AuNPs from the tumor. However, even 48 h post injection,

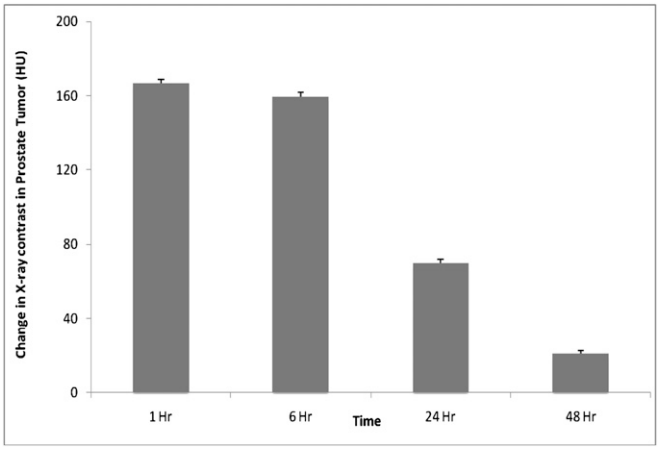

Fig. 4. A plot of change in CT numbers (in HUs) in prostate tumors in mice, preinjection and post injection of AuNP–BBN-3 (via i.p.) at various time points.

contrast agent was retained in the tumor. The targeting efficacy of AuNP–BBN-3 meets or exceeds the amount of gold that is required to induce x-ray contrast to function as a prostate-tumor-specific CT molecular imaging agent. The i.p. mode of administration of AuNP–BBN-3 conjugates affords optimal accumulation of AuNPs within the tumor, which is far superior to the i.v. mode of administration.

Conclusions

Our studies have shown that the surface chemistry of AuNPs accommodates prostate-tumor-specific bombesin peptide(s), thus achieving target specificity to deliver optimal payloads of AuNPs selectively at cancer receptor sites. GRP-receptor-specific targeted gold nanoparticles, as described here, will provide a plethora of opportunities toward the development of prostate-, breast-, or lung-tumor–specific gold nanoparticulate-based imaging and therapy agents. The hydrodynamic diameter of AuNP–BBN (115–155 nm) is optimally juxtaposed for effective penetration within tumor vasculature, which has porosity in the range of 150–300 nm. The interactions of AuNP–BBN with PC-3 cells ensue endocytosis within cells; thereby cellular imaging or cell-specific therapy will become feasible. Tumor/cell specificity of AuNPs will present a unique paradigm allowing labeling and internalization of diagnostic/therapeutic AuNPs within tumor cells for cell trafficking and tumor propagation—all aimed at gaining important insights into the complex tumor biology of metastasis.

Materials and Methods

Preparation of AuNP–BBN Nanoconjugates. The purified SAuNPs were used for conjugation with thioctic-acid-modified BBN with different ratios, e.g., AuNP: bombesin = 1:1, 1:2, and 1:3 for synthesizing AuNP–BBN-1, AuNP–BBN-2, and AuNP–BBN-3, respectively. For AuNP–BBN-1, 5.45 mg of BBN in 1 mL of HPLC-grade methanol was added to 5 mL of SAuNP solution (OD_{535} = 1.75). The mixture was stirred for 12 h at room temperature in a closed round-bottom flask. Reaction kinetics was monitored by the disk centrifuge technique. After successful conjugation, the AuNP–BBN-1 conjugates were washed three times with HPLC-grade water and three times with methanol to remove unbound peptide. The precipitate was finally dried under vacuum and characterized by UV, transmission electron microscope, differential centrifugal sedimentation, and dynamic light scattering techniques. A similar synthetic procedure was followed for the preparation of other conjugates, e.g., AuNP–BBN-2 and AuNP–BBN-3 where 10.92 and 16.27 mg of peptide in 1 mL of methanol was used to react with 5 mL of SAuNP solution, respectively.

Biodistribution of ^{198}AuNP–BBN-3 in Prostate-Tumor-Bearing SCID Mice. Prostate-tumor-bearing mice were developed by established protocols. The biodistribution of ^{198}AuNP–BBN-3 were assessed in five groups (five mice/group) of SCID (prostate tumor xenograft) mice weighing ~20 g. The animals were injected i.p. with ^{198}AuNP–BBN-3 (100 μL, 3.5 μCi) and killed after 30 min and 1, 2, 4, and 24 h. The amount of ^{198}AuNP in tumor, pancreas, kidney, spleen, lung, liver, and other organs was determined to assess the GRP receptors and tissue affinity. The amount of gold was estimated using scintigraphic techniques. A similar protocol was followed for determining the biodistribution of GA-^{198}AuNP in prostate-tumor-bearing mice.

AuNP–BBN-3 as Contrast Agent in CT Imaging of Prostate Cancer in Mice. Animals bearing a tumor mass of ~125 mg were used in this study. All animals were dosed with 100 μL of AuNP–BBN-3 dissolved in 1× PBS (3 mg/mL). Micro-CT was performed in all mice immediately before treatment and then 1, 6, 24, and 48 h after the start of treatment.

ACKNOWLEDGMENTS. We thank Dr. Silvia S. Jurisson (Department of Chemistry, University of Missouri) for providing helpful insights in radioanalytical chemistry, Dr. Timothy J. Hoffman and Gary L. Sieckman (Harry S. Truman Veterans Administration Medical Center) for in vitro cell affinity studies and EMC core (University of Missouri) for electron microscopy. This work was supported by grants from the National Institutes of Health (NIH)/National Cancer Institute under the Cancer Nanotechnology Platform program (Grant 5R01CA119412-01 and NIH 1R21CA128460-01 and NIH-Small Business Innovation Research Contract 241) and by the University of Missouri-Research Board Program C8761 RB 06-030.

1. Andriole GL, et al. (2009) Mortality results from a randomized prostate-cancer screening trial. *N Engl J Med* 360:1310–1319.
2. Morgan CL, Calkins RF, Cavalcanti EJ (1981) Computed tomography in the evaluation, staging, and therapy of carcinoma of the bladder and prostate. *Radiology* 140: 751–761.
3. Fournier G, Valeri A, Mangin P, Cussenot O (2004) Prostate cancer: Diagnosis and staging. (Translated from French) *Ann Urol (Paris)* 38:207–224.
4. Maio A, Rifkin MD (1995) Magnetic resonance imaging of prostate cancer: update. *Top Magn Reson Imaging* 7:54–68.
5. Turkbey B, Pinto PA, Choyke PL; Medscape (2009) Imaging techniques for prostate cancer: implications for focal therapy. *Nat Rev Urol* 6:191–203.
6. Dhar S, Gu FX, Langer R, Farokhzad OC, Lippard SJ (2008) Targeted delivery of cisplatin to prostate cancer cells by aptamer functionalized Pt(IV) prodrug-PLGA-PEG nanoparticles. *Proc Natl Acad Sci USA* 105:17356–17361.
7. Heath JR, Davis ME (2008) Nanotechnology and cancer. *Annu Rev Med* 59:251–265.
8. Chanda N, et al. (2009) Radioactive gold nanoparticles in cancer therapy: Therapeutic efficacy studies of GA-(198)AuNP-GA nanoconstruct in prostate tumor-bearing mice. *Nanomedicine* 6:201–209.
9. Chanda N, Shukla R, Katti KV, Kannan R (2009) Gastrin releasing protein receptor specific gold nanorods: Breast and prostate tumor avid nanovectors for molecular imaging. *Nano Lett* 9:1798–1805.
10. Huang HC, Barua S, Kay DB, Rege K (2009) Simultaneous enhancement of photothermal stability and gene delivery efficacy of gold nanorods using polyelectrolytes. *ACS Nano* 3:2941–2952.
11. Jain PK, Huang X, El-Sayed IH, El-Sayed MA (2008) Noble metals on the nanoscale: Optical and photothermal properties and some applications in imaging, sensing, biology, and medicine. *Acc Chem Res* 41:1578–1586.
12. Thaxton CS, et al. (2009) Nanoparticle-based bio-barcode assay redefines "undetectable" PSA and biochemical recurrence after radical prostatectomy. *Proc Natl Acad Sci USA* 106:18437–18442.
13. Hainfeld JF, Slatkin DN, Focella TM, Smilowitz HM (2006) Gold nanoparticles: A new X-ray contrast agent. *Br J Radiol* 79:248–253.
14. Kattumuri V, et al. (2007) Gum arabic as a phytochemical construct for the stabilization of gold nanoparticles: *In vivo* pharmacokinetics and X-ray-contrast-imaging studies. *Small* 3:333–341.
15. Kattumuri VCM, et al. (2006) Agarose-stabilized gold nanoparticles for surface-enhanced Raman spectroscopic detection of DNA nucleosides. *Appl Phys Lett* 88:153114.
16. Popovtzer R, et al. (2008) Targeted gold nanoparticles enable molecular CT imaging of cancer. *Nano Lett* 8:4593–4596.
17. Peer D, et al. (2007) Nanocarriers as an emerging platform for cancer therapy. *Nat Nanotechnol* 2:751–760.
18. Patra CR, et al. (2008) Targeted delivery of gemcitabine to pancreatic adenocarcinoma using cetuximab as a targeting agent. *Cancer Res* 68:1970–1978.
19. Reile H, Armatis PE, Schally AV (1994) Characterization of high-affinity receptors for bombesin/gastrin releasing peptide on the human prostate cancer cell lines PC-3 and DU-145: Internalization of receptor bound ^{125}I-(Tyr4) bombesin by tumor cells. *Prostate* 25:29–38.
20. De Vincentis G, et al. (2002) Phase I trial of technetium [Leu13] bombesin as cancer seeking agent: Possible scintigraphic guide for surgery? *Tumori* 88:S28–S30.
21. Scopinaro F, et al. (2003) ^{99m}Tc-bombesin detects prostate cancer and invasion of pelvic lymph nodes. *Eur J Nucl Med Mol Imaging* 30:1378–1382.
22. Gallant DJB, Bouchet B, Baldwin PM (1997) Microscopy of starch: Evidence of a new level of granule organization. *Carbohydr Polym* 32:177–191.
23. Gallant DJM, Mercier C, Guilbot, A (1972) Electron microscopy of starch granules modified by bacterial a-amylase. *Cereal Chem* 49:354–365.
24. Kannan R, et al. (2006) Nanocompatible chemistry toward fabrication of target-specific gold nanoparticles. *J Am Chem Soc* 128:11342–11343.
25. Maincent P, et al. (1992) Lymphatic targeting of polymeric nanoparticles after intraperitoneal administration in rats. *Pharm Res* 9:1534–1539.
26. Howard KA, et al. (2009) Chitosan/siRNA nanoparticle-mediated TNF-alpha knockdown in peritoneal macrophages for anti-inflammatory treatment in a murine arthritis model. *Mol Ther* 17:162–168.
27. Huang YH, et al. (2009) Nanoparticle-delivered suicide gene therapy effectively reduces ovarian tumor burden in mice. *Cancer Res* 69:6184–6191.
28. Sadauskas E, et al. (2007) Kupffer cells are central in the removal of nanoparticles from the organism. *Part Fibre Toxicol* 4:10.
29. Schuhmacher J, et al. (2005) GRP receptor-targeted PET of a rat pancreas carcinoma xenograft in nude mice with a ^{68}Ga-labeled bombesin(6-14) analog. *J Nucl Med* 46:691–699.
30. Montet X, Yuan H, Weissleder R, Josephson L (2006) Enzyme-based visualization of receptor-ligand binding in tissues. *Lab Invest* 86:517–525.
31. Smith CJ, et al. (2003) Radiochemical investigations of gastrin-releasing peptide receptor-specific [(99m)Tc(X)(CO)3-Dpr-Ser-Ser-Ser-Gln-Trp-Ala-Val-Gly-His-Leu-Met-(NH2)] in PC-3, tumor-bearing, rodent models: Syntheses, radiolabeling, and *in vitro/in vivo* studies where Dpr = 2,3-diaminopropionic acid and X = H2O or P(CH2OH)3. *Cancer Res* 63:4082–4088.
32. Durkan K, Lambrecht FY, Unak P (2007) Radiolabeling of bombesin-like peptide with ^{99m}Tc: ^{99m}Tc-litorin and biodistribution in rats. *Bioconjug Chem* 18:1516–1520.
33. Smith CJ, et al. (2003) Radiochemical investigations of ^{177}Lu-DOTA-8-Aoc-BBN[7-14] NH2: An *in vitro/in vivo* assessment of the targeting ability of this new radiopharmaceutical for PC-3 human prostate cancer cells. *Nucl Med Biol* 30:101–109.
34. Zhang G, et al. (2009) Influence of anchoring ligands and particle size on the colloidal stability and *in vivo* biodistribution of polyethylene glycol-coated gold nanoparticles in tumor-xenografted mice. *Biomaterials* 30:1928–1936.